

# An Image Processing Approach to Detection of Ridges and Ravines on Polygonal Surfaces

Alexander Belyaev and Yutaka Ohtake

The University of Aizu, Aizu-Wakamatsu, Fukushima 965-8580 Japan  
{belyaev, d8011101}@u-aizu.ac.jp

---

## Abstract

*Surface creases, ridges and ravines, provide us with important information about the shapes of 3D objects and can be intuitively defined as curves on a surface along which the surface bends sharply. Exploring similarity between edges of 2D grey-scale images and curvature extrema of 3D shapes and generalizing a basic edge detection approach to triangular meshes, we develop a method for detection of ridges and ravines on a smooth surface approximated by a triangular mesh. We also sketch three potential applications of our approach: mesh fairness evaluation, improving mesh decimation techniques, and simulating artistic pen-and-ink drawings of 3D objects.*

---

## 1. Introduction

Studying shapes of 3D objects we are interested in shape features which are invariant under rotations, translations, and scalings. Surface creases, ridges and ravines, curves on a surface along which the surface bends sharply, are among the most important such shape features.

Modern data-acquisition hardware is capable of producing high quality triangular meshes approximating accurately the surface geometry of physical objects. Surface features based on high-order surface derivatives can be extracted with reasonable accuracy. This opens up many new avenues for shape interrogation methods and, in particular, allows stable detection of surface creases defined via extrema of the principal curvatures along their curvature lines. Such extrema, as it is shown in the paper, are good for shape description and segmentation purposes, can be used for mesh fairness evaluation, have potential applications related to mesh decimation methods and simulating artistic pen-and-ink drawings of 3D objects.

**Contributions.** In this paper, we develop a method for detection of ridges and ravines defined via curvature extrema on a smooth surface approximated by a triangular mesh.

The method explores similarity between edges of 2D grey-scale images and curvature extrema of 3D shapes and generalizes a basic edge detection technique for triangle meshes.

We also sketch three potential applications of our approach: mesh fairness evaluation, improving mesh decimation techniques, and simulating artistic pen-and-ink drawings of 3D objects.

We discover new relationships between extrema of the principal curvatures along their curvature lines, extrema of the principal curvatures along their associated normal section curves, and curvature extrema of those normal section curves (see the last section of the paper appendix). It allows us to develop a numerical scheme for estimation of max/min of the principal curvatures along their curvature lines on a triangulated surface.

**Related work.** Our mathematical description of surface creases is based on study of extrema of the principal curvatures along their curvature lines. Besides the mathematical elegance of these surface features <sup>11, 20, 29, 13</sup> (a Nobel Prize laureate and a Fields medalist are among the authors of these works), some of them have been studied in connection with research on the accommodation of the eye lens <sup>11</sup>, structural geology <sup>30</sup>, segmentation of range images <sup>31, 4</sup>, image and data analysis <sup>39, 7, 13</sup>, face recognition <sup>10, 13</sup>, quality control of free-form surfaces <sup>16</sup>, analysis of satellite data and medical images <sup>24</sup>, and human perception <sup>15</sup>. The so-called crest lines <sup>25, 37</sup>, the loci of the maxima of the maximal absolute principal curvature (maximal in absolute value) along its curvature line, turned out to be anatomically meaningful and have been intensively studied in connection with research on the

anatomy of the human skull and brain<sup>28, 18</sup> (see also references therein). Surface line features defined via second order derivatives of the surface normal also have been used for shape segmentation purposes in<sup>17</sup>.

Practical extraction of the curvature extrema and their subsets involves estimation of high-order surface derivatives and, therefore, is not a simple task. Various numerical methods were proposed for surfaces given parametrically<sup>16, 14, 7</sup>, in implicit form<sup>26, 36, 37</sup>, or as the graph of a function defined on a rectangular grid (i.e., the grey-level intensity surface of a 2D image)<sup>31, 10, 24, 4</sup>.

Surprisingly, detection of curvature extrema on surfaces approximated by triangular meshes has received much less attention. In<sup>22</sup> a method to detect the extrema of the principal curvatures along their curvature lines on a triangulated surface was proposed. The method is based on a comparison of the areas of surface triangles and their corresponding triangles on the caustic (evolute, focal surface) generated by the curvature centers. The method has several drawbacks: it does not locate curvature extrema well, it requires a special attention near parabolic lines, and, the most important, it is unable to separate the curvature extrema along the curvature lines into the maxima and minima. A method to detect feature lines defined via second order derivatives of the surface normal on a triangulated surface was developed in<sup>17</sup>. However the geometry behind the method is not clear and, therefore, some doubts that the method is robust enough remain.

Image processing methods for extraction of curvature features on polygonal surfaces were used in<sup>17</sup> and<sup>23</sup>.

**A good definition for ridges and ravines and its motivation.** Let us define the *ridges* as the locus of points where the maximal principal curvature attains a positive maximum along its curvature line and the *ravines* as the locus of points where the minimal principal curvature attains a negative minimum along its curvature line.

This definition was originally introduced in<sup>1</sup> in an attempt to describe surface features corresponding to end points of the skeletons formed by the distance function singularities<sup>2</sup>. A equivalent definition was used in<sup>8</sup> (see also<sup>7</sup>).

Note that the term “ridges” is used in<sup>20, 29, 13</sup> to denote the extrema of the principal curvatures along their principal directions. However “ridge” sounds strange for the loci of points on a surface where the maximal (minimal) principal curvature takes a positive minimum (negative maximum) along its curvature line and the surface flattens.

The above definition of the ridges and ravines resembles a widely used definition for edges in image processing: the edges consists of pixels where the magnitude of the gradient of the image intensity has a local maximum in the direction of the gradient (see, for example,<sup>9</sup>).

Below we list several interesting properties of the ridges and ravines in order to motivate our definition.

The ridges and ravines are dual according to our definition: changing the surface orientation turns the ridges into the ravines and vice versa.

The crest lines are a subset of the union of the ridges and ravines.

The ridges and ravines are perceptually salient<sup>15</sup>. For a surface separating the space into two parts, ridge and ravine points correspond to the end points (the skeletal edge points according to the terminology used in<sup>38</sup>) of the medial axes (skeletons) of the parts. This beautiful relation between global (skeletons) and local (curvature extrema) surface features was probably first discovered in<sup>40</sup> and used for skeleton extraction in<sup>38</sup>. See also<sup>33</sup>.

An equivalent description of the ridges and ravines on a smooth generic surface can be given via cuspidal edges of the caustic generated by the surface normals. In<sup>3</sup> it was shown that the cuspidal edges of the caustic sheet associated with the maximal (minimal) principal curvature and pointing towards the surface correspond to the ridges (ravines).

The ridges and ravines can be also characterized via the contact between the surface and its spheres of curvature: the corresponding spheres of curvature have inner contacts with the surface at the ridge and ravine points.

Elementary proofs of these remarkable properties of the ridges and ravines are sketched in the appendix of the paper. Fig. 1 exposes some of these properties.

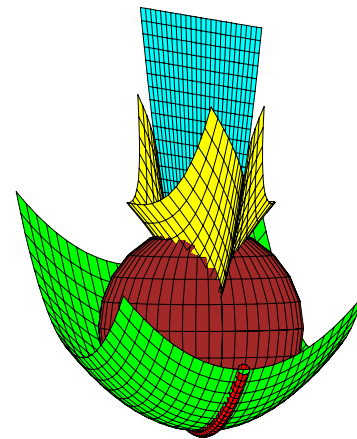


**Figure 1:** The elliptic paraboloid  $z = 3x^2 + y^2$  (green), its ridge (black), the caustic sheet (yellow) and the sphere of curvature (brown) associated with the maximal principal curvature at a ridge point, the skeleton (white).

In the rest of this paper we deal with triangular meshes approximating piecewise smooth surfaces accurately. In gen-

eral, a polygonal surface may have many pathological properties to compare with a piecewise smooth surface. Such pathological polygonal surfaces are not considered in this paper.

## 2. An image processing toolbox for extraction of ridges and ravines

Our algorithm to detect the ridges and ravines on a triangular mesh is simple and easy to implement. It resembles a standard edge detection procedure in image processing.

Since the ridges and ravines turn into each other as the surface orientation is changed, without loss of generality we can consider only the ridges.

**Curvature tensor estimation.** First we estimate the unit normal vector and the principal curvatures  $k_{\max}$  and  $k_{\min}$  together with their principal directions  $\mathbf{t}_{\max}$  and  $\mathbf{t}_{\min}$  at all the vertices. We use the method proposed in <sup>34</sup>.

**Nonmaximum suppression.** To decide whether  $k_{\max}$  attains a maximum along the normal section curve associated with  $\mathbf{t}_{\max}$  at a given vertex  $P$  we perform the following steps, see the left image of Fig. 2.

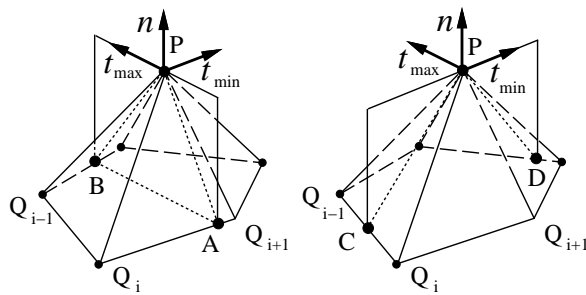


Figure 2:

1. Find the intersection between the normal section plane generated by  $\mathbf{t}_{\max}$  and  $\mathbf{n}$  and the polygon formed by the 1-ring neighbors  $Q_1, \dots, Q_m$  of  $P$ . Let the intersection consist of two points, say  $A$  and  $B$  (this is true for polygonal surfaces approximating piecewise smooth surfaces accurately). Let  $A$ , for example, belong to  $Q_i Q_{i+1}$ .
2. Interpolate the curvature values at  $A$  and  $B$ . For example, the curvature at  $A$  can be estimated by linear interpolating between the curvature values at  $Q_i$  and  $Q_{i+1}$ .
3. The maximal principal curvature attains a maximum at  $P$  along the normal section curve if  $k_{\max}(P)$ , the curvature at  $P$ , is greater than both  $k_{\max}(A)$  and  $k_{\max}(B)$ , the curvatures at  $A$  and  $B$ , respectively.

It turns out that estimation whether  $k_{\max}$  attains a maximum along its curvature line can be reduced to the above procedure

if we compare  $k_{\max}(P)$  with

$$k_{\max}(A) + \frac{1}{2(k_{\max}(P) - k_{\min}(P))} \left( \frac{\partial k_{\max}}{\partial \mathbf{t}_{\min}}(P) \right)^2 |PA|^2 \quad (1)$$

and

$$k_{\max}(B) + \frac{1}{2(k_{\max}(P) - k_{\min}(P))} \left( \frac{\partial k_{\max}}{\partial \mathbf{t}_{\min}}(P) \right)^2 |PB|^2 \quad (2)$$

instead of  $k_{\max}(A)$  and  $k_{\max}(B)$ , respectively. See the last section of the appendix for a proof. To estimate  $\partial k_{\max} / \partial \mathbf{t}_{\min}$  at  $P$  we find the intersection between the normal section plane generated by  $\mathbf{t}_{\min}$  and  $\mathbf{n}$  and the polygon  $Q_1, \dots, Q_m$ . Let the intersection consist of two points,  $C$  and  $D$ , see the right image of Fig. 2. The curvature values at  $C$  and  $D$  are also estimated by the linear interpolation. Now the curvature values  $k_{\max}(C)$ ,  $k_{\max}(P)$ , and  $k_{\max}(D)$  allow us to estimate  $\partial k_{\max} / \partial \mathbf{t}_{\min}$  at  $P$ .

We mark  $P$  as a ridge vertex if  $k_{\max}(P)$  is positive and greater than (1) and (2) simultaneously.

It turns out that extraction of curvature extrema along curvature lines (comparing  $k_{\max}(P)$  with (1) and (2)) is more stable numerically than extraction of curvature extrema along normal section curves (comparing  $k_{\max}(P)$  with  $k_{\max}(A)$  and  $k_{\max}(B)$ ) near umbilical points, see Fig. 3 below.

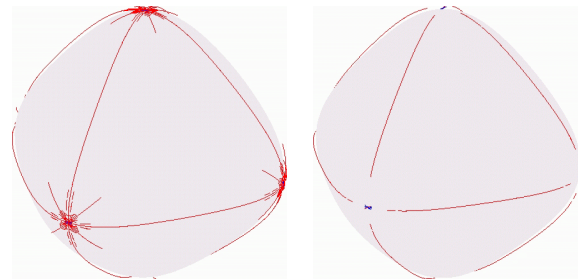


Figure 3: Positive maxima of the maximal principal curvature along its normal section curve (left) and curvature line (right) on a polygonal model of a rounded octahedron oriented by its inward normal.

Let us call the value of  $k_{\max}$  at a ridge vertex the strength of that ridge vertex. The above procedure produces many insignificant ridge vertices because of invisible defects of the triangulated surface. To reduce the number of those undesirable ridge vertices we add a thresholding operation. The idea is to keep only those ridge vertices whose strength is above some positive threshold:  $k_{\max} > T > 0$ .

**Hysteresis thresholding.** Following the analogy with the edge detection procedure, we use a thresholding idea introduced in <sup>5</sup>. We choose two thresholds  $T_{lo}$  and  $T_{hi}$  at the 30th and 60th percentiles of the ridge-strength data for the entire surface, i.e., the 30th percentile value is chosen so that for

30 percent of the surface vertices  $P$ ,  $k_{\max}(P)$  is below that value. We keep a chain of connected ridge vertices whose strength is above  $T_{lo}$  if the chain contains a ridge vertex with strength above  $T_{hi}$ .

Of course, the same hysteresis thresholding procedure can be applied separately to mesh parts with different geometry and the threshold can be selected according to local statistical properties of the surface.

**Visualization.** The ridge and ravine vertices can be visualized by attaching to them small segments directed along the tangents of the loci of curvature extrema along their curvature lines. However, computation of those tangents involves fourth-order surface derivatives (see the appendix) and, therefore, is very sensitive to noise. A better visualization effect is achieved by attaching small strokes directed along the principal directions. We use black strokes directed along  $t_{\min}$  to mark the ridge vertices and white strokes directed along  $t_{\max}$  to mark the ravine vertices. Some of our results are shown in Fig. 4.

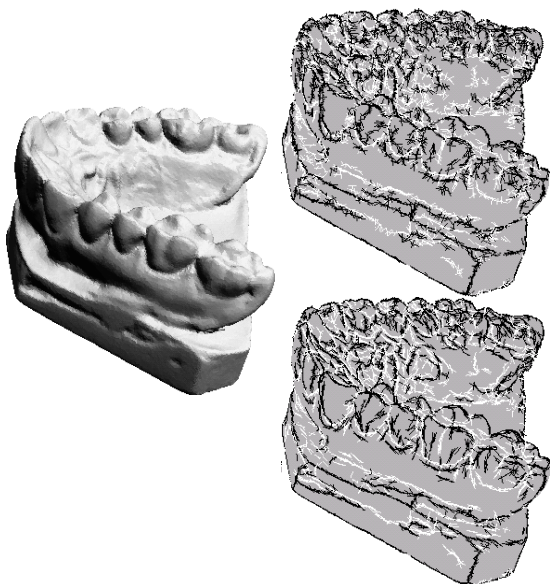


**Figure 4:** Left: the Teeth Casting model (courtesy Cyberware). Right: ridges (black) and ravines (white) obtained after nonmaximum suppression and filtering according to the 30/60% hysteresis thresholding rule. Top-right: the strokes are directed along the ridge and ravine directions. Bottom-right: the strokes are directed along the principal directions.

**Subtriangle-precision ridge detection.** To locate the ridge points more accurately we can enhance the nonmaximum suppression algorithm by the parabolic interpolation of  $k_{\max}$  along the polygonal line  $APB$ . If, for example, the parabola maximum is located over  $PA$  we consider the mesh triangle containing  $PA$  as a ridge triangle, see Fig. 5.

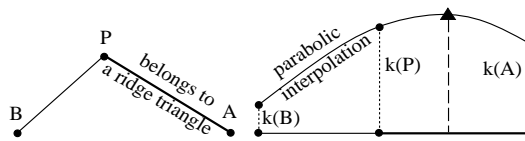


**Figure 5:**

**Morphology operations.** Even after hysteresis threshold filtering, the ridge and ravine mesh triangles form fragmentary patterns. We use simple dilation and erosion operations in order to reduce the fragmentation. First we add several layers of surrounding triangles. Then a simple thinning procedure is applied. Finally we remove the connected components of ridge triangles whose lengths are smaller than a given threshold. Fig. 6 demonstrates how our simple morphological scheme works.

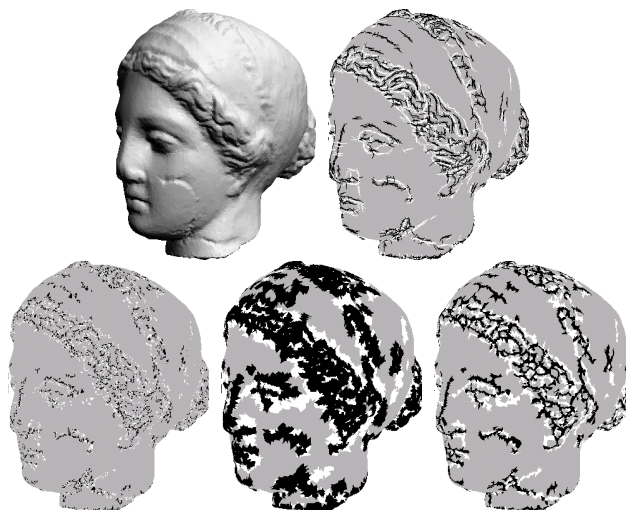


**Figure 6:** Top-left: the Venus model (courtesy Cyberware). Top-right: ridges and ravines are marked by the black and white strokes, respectively. Bottom: ridge and ravine triangles detected on the Venus model (left), after adding several layers of surrounding triangles (middle), after thinning (right).

**Smoothing.** Another way to remove insignificant ridge vertices is smoothing.

It seems natural to choose a smoothing procedure minimizing vertices drift over the surface. Among such smoothing schemes we mention those proposed in <sup>12</sup> and <sup>6</sup>. However, due to shrinkage, these smoothing schemes increase the mesh irregularity and, therefore, worsen curvature estimation. A method for smoothing without shrinkage was developed in <sup>35</sup>. It was reported in <sup>19</sup> that smoothing by the bilaplacian flow also produces satisfactory results.

Our smoothing scheme <sup>27</sup> described below combines together the discrete mean curvature flow proposed in <sup>6</sup> and the Laplacian flow.

Consider a discrete diffusion process acting on a surface mesh  $M$

$$\frac{\partial M}{\partial t} = D(M), \tag{3}$$

A discrete mean curvature flow acting on  $M$  is obtained from (3) by choosing  $D = Hn$  where  $H$  is a discrete approximation of the mean curvature and  $n$  is the unit normal consistent with the surface orientation.

The discrete mean curvature flow proposed in <sup>6</sup> increases mesh irregularity. To demonstrate this, let us consider the two-dimensional analog of the flow. Let  $r(s)$  be a plane curve parameterized by arclength parameter  $s$ . Consider three points on the curve

$$A = r(s - \alpha), \quad O = r(s), \quad B = r(s + \beta)$$

with distances  $a = |OA|$  and  $b = |OB|$  between them. Let  $r' = t$  and  $n = t^\perp$  compose the Frenet frame at  $O$ , see Fig. 7.

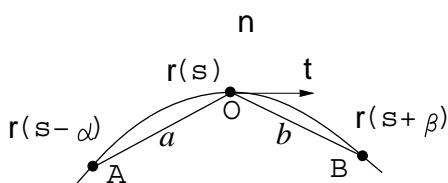


Figure 7:

The curvature vector  $kn$  is approximated by

$$-\frac{2}{a+b} \nabla(a+b) = \frac{2}{a+b} \left[ \frac{\vec{OA}}{a} + \frac{\vec{OB}}{b} \right] \tag{4}$$

Simple manipulations with Taylor series expansions and Frenet formulas show that (4) has the following expansion

$$n \left( k + \frac{b-a}{3} k' + O(a,b)^2 \right) + t \left( \frac{a-b}{4} k^2 + O(a,b)^2 \right),$$

where  $k'$  is the derivative of the curvature with respect to the arclength  $s$ .

If, for example, point  $O$  is located closer to  $A$  than to  $B$ , i.e.,  $b > a$ , then, due to the tangent components in the above expansion, one step of the discrete mean curvature flow shifts  $O$  closer to  $A$ .

Our idea is to compensate this undesirable effect by adding a tangent speed component to the mean curvature flow

$$\frac{\partial M}{\partial t} = Hn + St, \tag{5}$$

where  $t$  is a tangent vector to  $M$  and  $S$  is a function on  $M$ . Note that for a smooth surface adding a tangent speed component does not affect the geometry of the evolving surface.

Our implementation of (5) is as follows. Let us move every inner mesh vertex in the median direction (the direction defined by the simplest discrete Laplacian, the umbrella operator) such that the normal speed component is equal to the mean curvature at that vertex. More precisely, with a given vertex  $P$  let us associate the so-called umbrella operator <sup>19</sup>

$$U(P) = \frac{1}{n} \sum_i Q_i - P,$$

where vertices  $Q_1, \dots, Q_n$  form the first ring of neighbors of  $P$ . Let us define the median direction at  $P$  by  $m = U/\|U\|$  and let  $\theta$  be the angle between the mean curvature vector  $Hn$  and  $m$ ,  $\cos \theta = m \cdot Hn/|H|$ . Since the median direction vector  $m$  and the mean curvature vector  $Hn$  may have opposite normal components (i.e.,  $\theta > \pi/2$ ) at saddle vertices, see Fig. 8b, we use the smoothing flow defined by the following vertex update rule

$$P_{new} \leftarrow P_{old} + \tau \hat{D}(P_{old}), \tag{6}$$

where  $\tau$  is a small time step-size parameter, the diffusion operator  $\hat{D}$  is given by

$$\hat{D} = \begin{cases} \frac{|H|m}{\cos \theta} & \text{if } \cos \theta > \varepsilon \\ 2Hn - \frac{|H|m}{\cos \theta} & \text{if } \cos \theta < -\varepsilon \\ 0 & \text{if } |\cos \theta| \leq \varepsilon \end{cases}$$

and the geometric idea behind it is presented in Fig. 8.

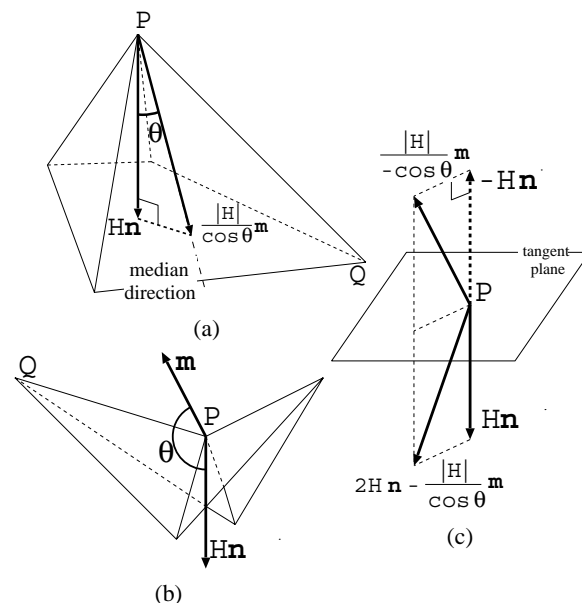
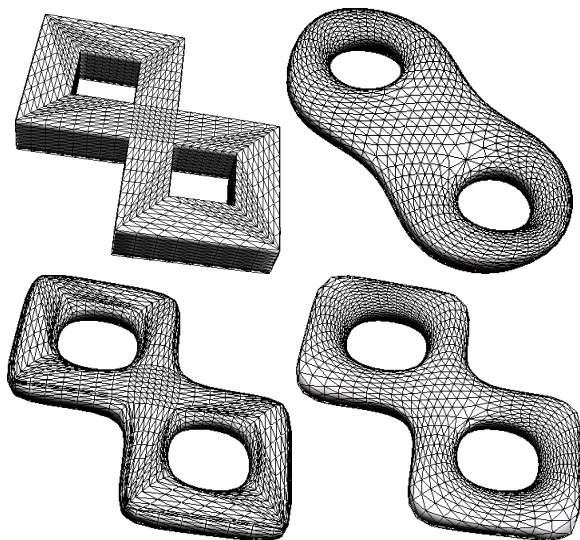


Figure 8: (a) The median and normal vectors lie on the same side from the tangent plane: moving in the median direction with normal speed component equal to the mean curvature. (b) The median and normal vectors lie on the opposite sides from the tangent plane may happen for saddle vertices. (c) Computation of the speed vector in (b).



**Figure 9:** *Top-left: a polygonal two-holed torus consisting of parts with different sampling rates. Top-right: Laplacian smoothing improves the mesh sampling rate but substantially deforms the initial shape. Bottom-left: the mean curvature flow<sup>6</sup> increases mesh irregularity. Bottom-right: smoothing according to (6) produces a regular meshing surface whose shape is close to the shape produced by the mean curvature flow.*

Here  $\epsilon$  is a small positive number. According to our experience, choosing  $\epsilon = 0.1$  produces good results in smoothing polygonal objects of various complexity.

See Fig. 9 where our smoothing scheme is tested on a two-holed torus.

Our modification of the mean curvature flow equalizes the mesh sampling rate quickly and, therefore, allows us to achieve stable estimates of the principal curvatures and directions on the smoothed mesh.

**Gathering all together.** Our complete scheme for ridge and ravine detection on a triangulated surface combines together the previous steps in the following order:

- smooth the surface;
- estimate the principal curvatures and principal directions at every vertex of the smoothed surface;
- detect the ridge and ravine vertices on the smoothed surface using nonmaximum suppression and hysteresis thresholding;
- detect the ridge and ravine mesh triangles using the subtriangle-precision operation;
- apply morphology operations to reduce the fragmentation of the ridges and ravines;
- place the ridges and ravines on the original surface.

The top row of Fig. 10 demonstrates various stages of our algorithm applied to the Stanford bunny model. The first image of the bottom row shows the final result obtained while using (6) for smoothing. Other images of the bottom row demonstrate ridge and ravine extraction results after employing various smoothing methods.

The choice of a smoothing method is crucial. Different smoothing schemes may produce different ridge and ravine patterns. What smoothing procedure is the best one is not clear and we leave it as a theme for future research.

### 3. Potential applications

We believe that potential applications of our technique for extraction of surface creases are various and many. Below we sketch only three of them, mesh fairness evaluation, mesh decimation, and simulating artistic pen-and-ink drawings of 3D objects.

**Mesh fairness evaluation.** In various engineering applications, surfaces with a high degree of “fairness” are required. The concept of fairness is typically associated with curvature characteristics of a surface. A fair surface has smoothly varying curvatures. Thus the pattern of ridges and ravines on a smooth surface is very useful for evaluation of the surface fairness. As we see, the ridges and ravines are very sensitive to even small shape irregularities and can be used for fairness evaluation.

#### Simulating artistic pen-and-ink drawings of 3D objects.

Simulating pen-and-ink drawings is an area of intensive research (see, for example, <sup>32</sup> and references therein). Our technique to visualize the ridge and ravine vertices by attaching at them small strokes directed along the principal directions turns out to be useful for simulating artistic sketching of 3D objects, see Fig. 11.

Of course, using curved strokes with varying lengths and widths will provide with better simulating artistic pen-and-ink drawings.

An incomplete mathematical explanation of why the ridges and ravines are good for simulating artistic drawings of 3D objects can be found in <sup>39</sup>. Consider a grey-scale image of an illuminated 3D object. Under general illumination and reflection conditions, the zero-crossings of the second directional derivative of the image intensity along the direction of the image intensity gradient occur near the extrema of the principal curvature along their principal directions. It remains to recall that the edges of a grey scale image are usually defined as sets of pixels where the magnitude of the gradient of the image intensity has a local maximum in the direction of the gradient.

**Mesh decimation.** The goal of the decimation of a polygonal mesh is to reduce the total number of the polygons (mesh

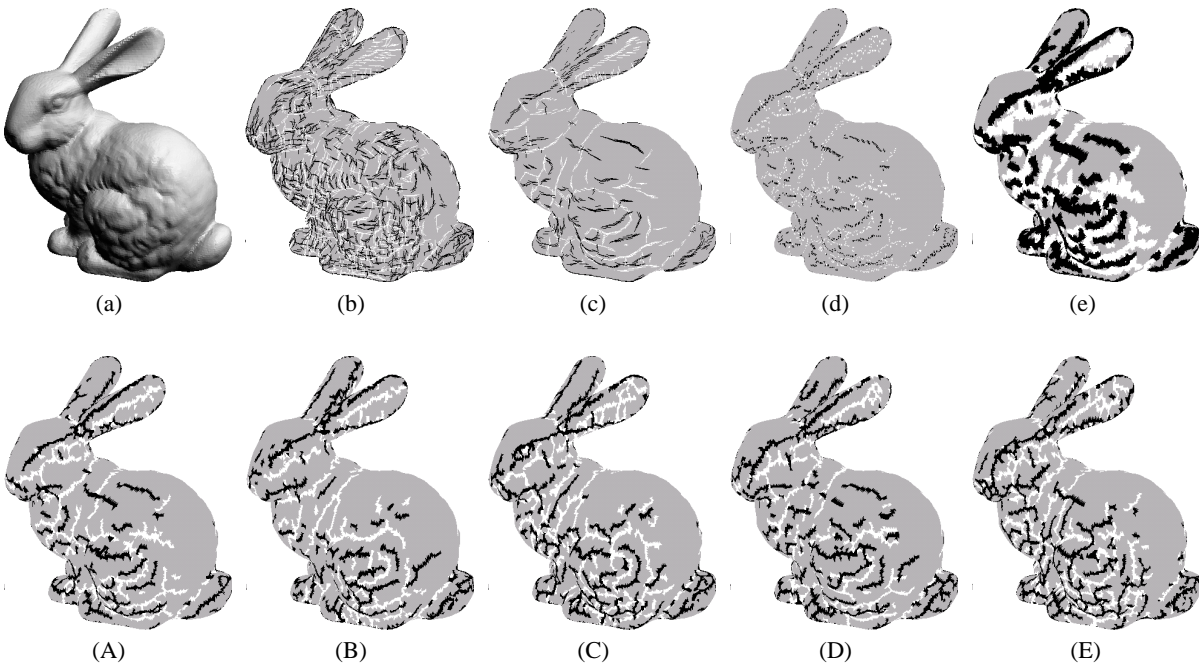


**Figure 10:** (a) The Stanford bunny. (b) The ridges and ravines detected on the bunny are marked by the black and white strokes, respectively; the 30/60% hysteresis thresholding rule was applied. (c) The same as (b) on the bunny smoothed according to our scheme (6). (d) The ridge and ravine triangles are marked on the smoothed bunny. (e) Several layers of the surrounding triangles are added to every ridge and ravine triangle. (A) Final result after thinning. (B) Smoothing by the bilaplacian flow was used. (C) Smoothing by the Taubin method<sup>35</sup> was used. (D) Smoothing by the mean curvature flow<sup>6</sup> was used. (E) Smoothing by the Guskov method<sup>12</sup> was used.

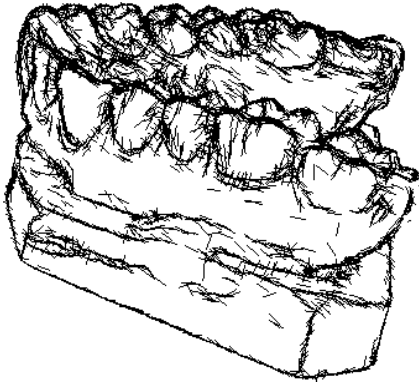


**Figure 11:**

faces) while providing a good approximation of the original geometry. A useful idea is to keep certain feature edges and vertices representing important geometric properties of the mesh fixed during a decimation procedure. This idea was implemented in<sup>21</sup> where the feature edges and vertices were detected automatically as the edges whose dihedral angle is

below a certain threshold and as the vertices whose curvature is above a certain threshold.

Instead of keeping the feature edges and vertices fixed, let us keep the ridge and ravine vertices fixed during a decimation procedure. However the straightforward implementation of this idea produces acute triangles near ridge and ravine vertices. To avoid acute triangles, we increase the number of fixed vertices with every decimation iteration such that the front of fixed vertices propagates from the ridges and ravines.

In Fig. 12 we present our decimation experiments with two surfaces having different geometry. The models exposed in Fig. 12c consist of much less triangles than the original models shown in Fig. 12a but look very close to them.

#### 4. Conclusions and future work

We have shown how basic image processing tools used for detection of edges in 2D grey-scale images can be extended to detection of ridges and ravines on a surface given by a triangular mesh. We have also outlined three potential applications of our approach: mesh quality evaluating, improving mesh decimation techniques, and simulating artistic pen-and-ink drawings of 3D objects.

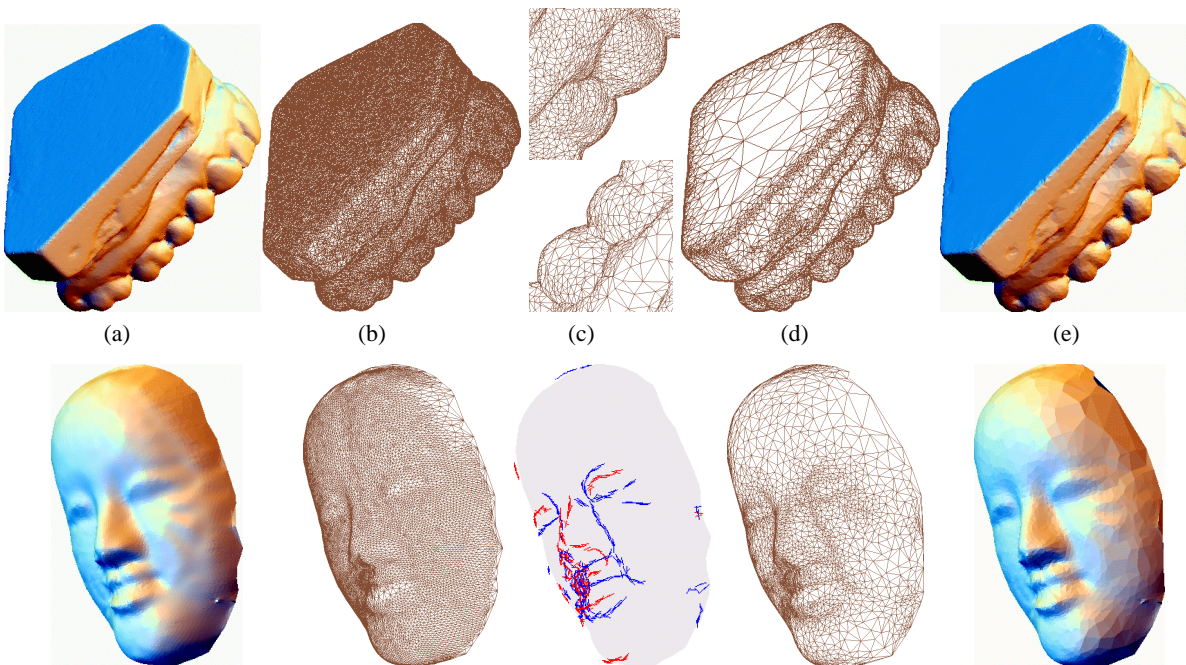


**Figure 12:** Top row: (a) the Teeth Casting model; (b) its wireframe image; (c) a magnified view of a part of the mesh before (top) and after (bottom) decimation; (d) a wireframe image of the model after decimation; (e) the decimated model. Bottom row: (a) a Noh mask model; (b) its wireframe image; (c) ridges and ravines detected on the model; (d) a wireframe image of the Noh mask model after decimation; (e) the decimated model. The models are flat-shaded to enhance the faceting effect.

Many directions for future work remain. It concerns every step of our algorithm for ridge and ravine detection. Another hysteresis thresholding scheme can be developed if, additionally, we take into account hierarchal relations between curvature extrema along the curvature lines, curvature extrema along the normal section curves associated with the principal directions, and the curvature extrema of the normal section curves (see the last section of the appendix). Our implementation of morphological operations is very primitive and can be substantially improved. As we already noted in the main part of the paper, choosing a proper smoothing scheme requires a further study.

Finally, we have only sketched three possible applications of our approach. Deeper treatments of them are also themes for future research.

## References

1. E. V. Anoshkina, A. G. Belyaev, and T. L. Kunii. Detection of ridges and ravines based on caustic singularities. *Int. J. Shape Modeling*, 1(1):13–22, 1994. 2
2. E. V. Anoshkina, O. G. Belyaev, A. G. Okunev, and T. L. Kunii. Ridges and ravines: a singularity approach. *Int. J. Shape Modeling*, 1(1):1–12, 1994. 2
3. A. G. Belyaev, E. V. Anoshkina, and T. L. Kunii. Ridges, ravines, and singularities. In A. T. Fomenko, and T. L. Kunii, *Topological Modeling for Visualization*. Ch. 18, pages 375–383, Springer, 1997. 2, 9
4. A. G. Belyaev, I. A. Bogaevski, and T. L. Kunii. Ridges and ravines on a surface and segmentation of range images. In *Vision Geometry VI, Proc. SPIE 3168*, pages 106–114, 1997. 1, 2
5. J. Canny. A computational approach to edge detection. *IEEE Transactions on Pattern Analysis and Machine Intelligence*, 8(6):679–698, 1986. 3
6. M. Desbrun, M. Meyer, P. Schröder, and A. H. Barr. Implicit fairing of irregular meshes using diffusion and curvature flow. *Proc. SIGGRAPH 99*, pages 317–324, 1999. 4, 5, 6, 7
7. D. Eberly. *Ridges in Image and Data Analysis*. Kluwer, 1996. 1, 2
8. D. Eberly, R. Gardner, D. Morse, S. Pizer, and C. Scharlach. Ridges for image analysis. *J. Mathematical Imaging and Vision*, 4(4):353–373, 1994. 2
9. O. Faugeras. *Three-Dimensional Computer Vision*, Ch. 4: *Edge Detection*. MIT Press, 1993. 2
10. G. G. Gordon. Face recognition from depth maps and surface curvature. In *Geometric Methods in Computer Vision, Proc. SPIE 1570*, pages 234–247, 1991. 1, 2
11. A. Gullstrand. Zur kenntnis der kreispunkte. *Acta Mathematica*, 29:59–100, 1904. 1

12. I. Guskov, W. Sweldens, and P. Schröder. Multiresolution signal processing for meshes. *Proc. SIGGRAPH 99*, pages 325–334, 1999. 4, 7
13. P. L. Hallinan, G. G. Gordon, A. L. Yuille, P. Giblin, and D. Mumford. *Two- and Tree-Dimensional Patterns of the Face*. Ch. 6: *Parabolic Curves and Ridges on Surfaces*. A K Peters, 1999. 1, 2, 9
14. E. Hartmann. On the curvature of curves and surfaces defined by normalforms. *Comput. Aided Geom. Design*, 16(5):355–376, 1999. 2
15. D. D. Hoffman and W. A. Richards. Parts of recognition. *Cognition*, 18:65–96, 1985. 1, 2
16. M. Hosaka. *Modeling of Curves and Surfaces in CAD/CAM*. Springer, Berlin, 1992. 1, 2
17. J. Hoschek, U. Dietz, and W. Wilke. A geometric concept of reverse engineering of shape: Approximation and feature lines. In M. Dæhlen, T. Lyche, and L. L. Schumaker, editors, *Mathematical Methods for Curves and Surfaces II*, pages 319–326. Vanderbilt Univ. Press, 1998. 2
18. N. Khaneja, M. I. Miller, and U. Grenader. Dynamic programming generation of curves on brain. *IEEE Transactions on Pattern Analysis and Machine Intelligence*, 20(11), 1998. 2
19. L. Kobbelt, S. Campagna, J. Vorsatz, and H.-P. Seidel. Interactive multiresolution modeling on arbitrary meshes. In *Proc. SIGGRAPH 98*, pages 105–114, 1998. 4, 5
20. J. J. Koenderink. *Solid Shape*. MIT Press, 1990. 1, 2
21. A. Lee, W. Sweldens, P. Schröder, and D. Dobkin. Maps: Multiresolution adaptive parametrization of surfaces. *Proc. SIGGRAPH 98*, pages 95–104, 1998. 7
22. G. Lukács and L. Andor. Computing natural division lines on free-form surfaces based on measured data. In M. Dæhlen, T. Lyche, and L. L. Schumaker, editors, *Mathematical Methods for Curves and Surfaces II*, pages 319–326. Vanderbilt Univ. Press, 1998. 2
23. A. P. Mangan and R. T. Whitaker. Partitioning 3D surface meshes using watershed segmentation. *IEEE Trans. on Visualization and Computer Graphics*, 5(4):308–321, 1999. 2
24. O. Monga, N. Armande, and P. Montesinos. Thin nets and crest lines: Application to satellite data and medical images. *Computer Vision and Image Understanding: CVIU*, 67(3):285–295, 1997. 1, 2
25. O. Monga, N. Ayache, and P. T. Sander. From voxel to intrinsic surface features. *Image and Vision Computing*, 10(6):403–417, 1992. 1
26. O. Monga and S. Benayoun. Using partial derivatives of 3d images to extract typical surface features. *Computer Vision and Image Understanding: CVIU*, 61:171–189, 1995. 2
27. Yu. Ohtake, A. G. Belyaev, and I. A. Bogaevski. Polyhedral surface smoothing with simultaneous mesh regularization. In *Geometric Modeling & Processing 2000*, pages 229–237, Hong Kong, April 2000. 5
28. X. Pennec, N. Ayache, and J. P. Thirion. Landmark-based registration using features identified through differential geometry. In I. N. Bankman, editor, *Handbook of Medical Imaging*. Academic Press, 2000. 2
29. I. R. Porteous. *Geometric Differentiation for the Intelligence of Curves and Surfaces*. Cambridge University Press, Cambridge, 1994. 1, 2
30. J. G. Ramsay. *Folding and Fracturing of Rocks*. McGraw Hill, 1967. 1
31. P. Saint-Marc and G. Medioni. Adaptive smoothing for feature extraction. In *Proc. DARPA Image Understanding Workshop*, pages 1110–1113, Cambridge, Massachusetts, 1988. 1, 2
32. M. P. Salisbury, M. T. Wong, J. F. Hughes, and D. H. Salesin. Orientable textures for image-based pen-and-ink illustrations. In *Proc. SIGGRAPH 97*, pages 401–406, 1997. 6
33. E. C. Sherbrooke, N. M. Patrikalakis, and F.-E. Wolter. Differential and topological properties of medial axis transform. *Graphical Models and Image Processing*, 58(6):574–592, 1996. 2
34. G. Taubin. Estimating the tensor of curvature of a surface from a polyhedral approximation. In *Proc. ICCV'95*, pages 902–907, 1995. 3
35. G. Taubin. A signal processing approach to fair surface design. In *Proc. SIGGRAPH 95*, pages 351–358, 1995. 4, 7
36. J.-P. Thirion and A. Gourdon. The 3d marching lines algorithm. *Graphical Models and Image Processing*, 58(6):503–509, 1996. 2
37. J.P. Thirion. The extremal mesh and the understanding of 3d surfaces. *IJCV*, 19(2):115–128, 1996. 1, 2
38. G.M. Turkiyyah, D.W. Storti, M. Ganter, H. Chen, and M. Vismawala. An acceleration triangulation method for computing the skeletons of free-form solid models. *Computer-Aided Design*, 29(1):5–19, 1997. 2
39. A.L. Yuille. Zero crossings on lines of curvature. *Graphical Models and Image Processing*, 45(1):68–87, 1989. 1, 6
40. A.L. Yuille and M. Leyton. 3d symmetry-curvature duality theorems. *Graphical Models and Image Processing*, 52(1):124–140, 1990. 2

## Appendix

The purpose of this appendix is to sketch elementary proofs of the properties of the curvature extrema that we have mentioned and used in the main part of the paper. The mathematics which we employ here consists of Taylor series manipulations. Most of the material presented below can be found in <sup>3</sup> and <sup>13</sup>. The last section contains new results.

Consider a smooth generic surface. Denote by  $k_{\max}$  and  $k_{\min}$  the largest and the smallest principal curvatures, respectively,  $k_{\max} \geq k_{\min}$ . For a given non-umbilic point  $P$  on the surface let us choose coordinates in the space so that  $P$  is at the origin, the  $(x, y)$ -plane is the tangent plane to the surface at  $P$ , the principal directions  $t_{\max}$  and  $t_{\min}$  coincide with  $x$  and  $y$  axes, respectively, and the normal  $n$  coincides with  $z$ -axis. Then the surface is expressible in the Monge form as the graph of a generic smooth function  $z = F(x, y)$ , where

$$F(x, y) = \frac{1}{2} (\lambda x^2 + \mu y^2) + \frac{1}{6} (ax^3 + 3bx^2y +$$

$$+ 3cxy^2 + dy^3) + \frac{1}{24}(ex^4 + 4fx^3y + \dots) + O(x,y)^5$$

with  $\lambda = k_{\max}(0,0)$ ,  $\mu = k_{\min}(0,0)$ ,  $\lambda > \mu$ .

The Taylor series expansion of  $k_{\max}$  at  $P$  has the form

$$k_{\max}(x,y) = \lambda + ax + by + O(x,y)^2.$$

Since the vectors  $(1,0)$  and  $(0,1)$  represent  $\mathbf{t}_{\max}$  and  $\mathbf{t}_{\min}$  at  $P$ , respectively, then

$$\frac{\partial k_{\max}}{\partial \mathbf{t}_{\max}}(0,0) = a \quad \frac{\partial k_{\max}}{\partial \mathbf{t}_{\min}}(0,0) = b \quad (7)$$

Below we will use frequently the function  $e_{\max} = \partial k_{\max} / \partial \mathbf{t}_{\max}$ . The extrema of the maximal principal curvature along its curvature line are given in the implicit form by the zero-crossings of  $e_{\max}$ .

We call the intersection between the surface and the normal plane generated by the normal  $\mathbf{n}$  and a tangent  $\mathbf{t}$  by the *normal section curve* associated with  $\mathbf{t}$ .

Let the surface orientation be chosen so that the maximal principal curvature is strictly positive at  $P$

$$k_{\max}(0,0) > 0.$$

**Ridges.** The curvature line associated with  $k_{\max}$  is locally described by the problem

$$\frac{dy}{dx} = \frac{bx + cy}{\lambda - \mu} + O(x,y)^2, \quad y(0) = 0.$$

Therefore,  $y'(0) = 0$ ,  $y''(0) = b/(\lambda - \mu)$  and in a neighborhood of the origin the curvature line is approximated by the parabola

$$y = \frac{bx^2}{2(\lambda - \mu)}.$$

It allows to compute the Taylor series expansion of  $k_{\max}$  at the origin along the associated curvature line

$$\lambda + ax + \left(-3\lambda^3 + e + \frac{3b^2}{\lambda - \mu}\right) \frac{x^2}{2} + O(x^3) \quad (8)$$

Analyzing asymptotic expansion (8) we obtain that  $P$  is a generic ridge point (the maximal principal curvature has a positive maximum along its curvature line) iff

$$\lambda > 0, \quad a = 0, \quad A = -3\lambda^3 + e + \frac{3b^2}{\lambda - \mu} < 0. \quad (9)$$

Note that

$$A = \frac{\partial e_{\max}}{\partial \mathbf{t}_{\max}}(0,0) = \frac{d^2 k_{\max}}{ds_{\max}^2}(0,0),$$

where  $s_{\max}$  is the arclength of the curvature line associated with  $k_{\max}$ .

If  $P$  is a ridge point, the tangent direction to the ridge at  $P$  is given by  $\{Ax + By = 0, z = 0\}$ , where

$$A = \frac{\partial e_{\max}}{\partial \mathbf{t}_{\max}}(0,0) \quad \text{and} \quad B = \frac{\partial e_{\max}}{\partial \mathbf{t}_{\min}}(0,0) = f + \frac{3bc}{\lambda - \mu}.$$

**Contact with osculating spheres.** Let us consider the loci of points where the curvature of the intersection curve between the surface and the plane  $\{y = \alpha z\}$ , where  $\alpha$  is a parameter. The intersection curve between the surface and the plane is locally described by

the equation  $y = \alpha\lambda x^2/2 + \dots$ . The Taylor expansion of the curvature of the curve is the product of  $\sqrt{1 + \alpha^2}$  and

$$\lambda + ax + \left(-3\lambda^3(1 + \alpha)^2 + 3\lambda^2\mu\alpha^2 + 6b\lambda\alpha^2 + e\right) \frac{x^2}{2} + O(x^3) \quad (10)$$

Thus, if the origin is a ridge point ( $a = 0$ ), the type of the extremum of the curvature at the origin is defined by the sign of

$$-3\lambda^3(1 + \alpha)^2 + 3\lambda^2\mu\alpha^2 + 6b\lambda\alpha^2 + e.$$

This expression is a quadratic polynomial in  $\alpha$ . The discriminant is given by

$$D = 3\lambda^2(\lambda - \mu)A.$$

Now from (8) it follows that the osculating spheres (spheres of curvature) associated with  $k_{\max}$  have inner contacts with the surface at the ridge points.

**Ridges and caustic ribs.** The intersection between the caustic sheet associated with  $k_{\max}$  and the plane  $\{y = 0\}$  gives a curve described locally by

$$x = -\frac{A}{3\lambda}t^3 + O(t^4), \quad z = \frac{1}{\lambda} - \frac{A}{2\lambda^2}t^2 + O(t^3).$$

At a neighborhood of the point  $(0,0,1/\lambda)$  the intersection curve is locally a semicubical parabola. Thus the cuspidal edges (ribs) of the caustic sheet associated with  $k_{\max}$  and pointing towards the surface correspond to the ridges.

**Ridges via normal sections.** Let us consider the function

$$K(x,y) = k_{\max}(x,y) + \frac{C}{2}(x^2 + y^2 + F(x,y)^2)$$

obtained from the maximal principal curvature by adding a function proportional to the squared distance from the origin. The Taylor series expansion of the restriction of  $K(x,y)$  onto the normal section associated with  $\mathbf{t}_{\max}$  has the form

$$\lambda + ax + \left(-3\lambda^3 + e + \frac{2b^2}{\lambda - \mu} + C\right) \frac{x^2}{2} + O(x^3) \quad (11)$$

Choosing  $C = b^2/(\lambda - \mu)$  one can detect the ridge points as positive maxima of  $K(x,y)$  along the normal section associated with  $\mathbf{t}_{\max}$ . Similarly, choosing  $C = -2b^2/(\lambda - \mu)$  one can detect the loci of points where the curvature of the normal section associated with  $\mathbf{t}_{\max}$  has a local positive maximum (see (10) with  $\alpha = 0$ ).

From (8) and (11) with  $C = 0$  it follows that the ridges are a subset of the loci of points where  $k_{\max}$  has a positive maximum along the normal section associated with  $\mathbf{t}_{\max}$ . Both these families of curves do not pass through the generic umbilics since the term  $b^2/(\lambda - \mu)$  dominates in (8) and (11) near a generic umbilic. Therefore, the curves do not have branch points on a generic smooth surface. Moreover, both the families are a subset of the loci of points where the curvature of the normal section associated with  $\mathbf{t}_{\max}$  has a local positive maximum.